Environmental Science Nano

Effect of Calcination Temperature on Neptunium Dioxide Microstructure and Dissolution

Journal:	*Environmental Science: Nano*
Manuscript ID	EN-ART-07-2020-000689.R2
Article Type:	Paper

Environmental Impact Statement

Neptunium-237 is a long-lived radioisotope and a risk-driver during the subsurface disposition of nuclear materials due to its high mobility and acute radiotoxicity. The solubility of neptunium dioxide ($NpO_2(s)$) is a key measurement for environmental fate and transport given that oxides are a common actinide storage and disposition waste form. Reported solubilities of actinide dioxide solids vary by orders of magnitude without sufficient explanation. In this work, dissolution experiments supported by high resolution microscopy (previously unreported) suggest that variations in solubility stem from differences in free energy driven by calcination temperature and resultant particle size of the material.

EFFECT OF CALCINATION TEMPERATURE ON NEPTUNIUM DIOXIDE MICROSTRUCTURE AND DISSOLUTION

Kathryn M. Peruski[(1)*] *and Brian A. Powell*[(1,2,3)*]

[(1)]Environmental Engineering and Earth Sciences, Clemson University, Anderson, SC, US 29625

[(2)]Department of Chemistry, Clemson University, Clemson, SC USA 29634

[(3)]Savannah River National Laboratory, Aiken, SC, USA 29808

KEYWORDS: Neptunium dioxide, solubility, particle size, actinides

ABSTRACT:

Comprehensive thermodynamic understanding of nuclear materials is paramount for long-term management of legacy nuclear waste and commercial spent nuclear fuel. Actinide oxides ($AnO_2(s)$) are ubiquitous materials throughout the nuclear fuel cycle, yet existing thermodynamic data has noticeable discrepancies, creating uncertainty in environmental prediction of the fate of nuclear materials. The microstructure of actinide oxides, particularly neptunium (Np) and plutonium (Pu), is rarely investigated using high resolution electron microscopy, but such features may illuminate why differences in solubility measurements persist. The aim of this study was to synthesize $NpO_2(s)$ at varying calcination temperatures, characterize the materials using high resolution electron microscopy, and perform batch solubility studies to measure total dissolved Np as a function of calcination temperature. The current work demonstrates the sizable differences in dissolution of $NpO_2(s)$ based on process conditions, such as the temperature at which the material is calcined and resultant particle size, and the need for more thorough evaluation of the microstructure of solid phases used to generate thermodynamic data of actinides.

Introduction

Proposed geologic disposal of commercial spent nuclear fuel, along with ongoing management of legacy nuclear waste, necessitates prediction of environmental fate and transport of actinide solid phases, which comprise a majority of long-lived nuclear waste products. Actinide dioxides ($AnO_2(s)$) are key solid phases throughout the nuclear fuel cycle. Commercial spent nuclear fuel is primarily composed of uranium dioxide ($UO_2(s)$), with other actinide dioxides, including plutonium and neptunium dioxide ($PuO_2(s)$ and $NpO_2(s)$, respectively), present as substitutions in the polycrystalline fuel grain matrix[1, 2]. Dioxides are also commonly used as stable storage forms for $PuO_2(s)$ and $NpO_2(s)$ due to their predicted thermodynamic stability. Given their ubiquity throughout the nuclear fuel cycle and profound insolubility[3-7], actinide dioxides are considered an important and solubility limiting solid phase for prediction of environment fate and transport of actinides.

Reported aqueous solubility data for actinide oxides vary by orders of magnitude[3, 5] but reason for such variation has not been adequately explained. Particle size and nanocrystalline solid phases[5, 6], as well as amorphous hydroxide or hydrous

oxide phases[3, 8], have been proposed as potential sources of discrepancy in aqueous solubility data sets. The current work hypothesizes that such discrepancies are due to surface energy effects in nanocrystalline actinide dioxides. This hypothesis is supported by recent advances in high temperature melt calorimetry[9-11], which have allowed for measurement of surface energy of metal oxide materials, including iron[12], zirconium[13], titanium[13], manganese[14], and uranium[15] oxides, indicating that phases considered to be metastable are actually thermodynamically stable as nanograined solids. As such, nanograined solids with high surface energy may persist, rather than coarsening to lower free energy states, due to spatial or kinetic constraints[13]. While inconsistencies between actinide dioxide solubility data sets are acknowledged throughout the literature, lack of advanced solid phase characterization, particularly imaging of actinide dioxide particle morphology and texture, makes it difficult to validate hypotheses for sources of variability. Solid phases used in actinide solubility studies are typically amorphous hydrous oxides or hydroxides[3], rather than pure, crystalline dioxides. Precipitation of these materials is achieved through low temperature alkaline hydrolysis, where acidic Np(IV) stock solutions are rapidly neutralized using NaOH to

pH values of 8-10[4, 7, 16-19]. More recent advances in actinide characterization techniques have revealed that such precipitates are nanocrystalline solids[20, 21]. With the advancement in solid phase characterization techniques for actinide materials, it is possible to identify if the reactivity differences observed in other metal oxides for nanograined solids are also present for nanograined transuranic oxides.

Crystalline actinide dioxides are reliably produced through oxalate precipitation and subsequent calcination, which has been the standard method since the 1960s when it was first employed for both Np and Pu[22, 23]. Early work on actinide oxalates and subsequent oxide conversion varied oxalate precipitation parameters as well as calcination temperature to achieve ideal product for storage and transportation of nuclear materials. This method was originally optimized for high chemical yield of actinides, low moisture adsorption, and particle size[24-27]. Oxalate morphology can be altered through variation of initial precipitation parameters (pH, concentration of actinide stock, stirring speed, addition rate)[24-29], but most studies suggest that morphology is preserved during calcination and that surface area and particle size both decrease during calcination[24, 30]. Given the age of the initial studies, electron microscopy

techniques were limited, and published electron micrographs are on the scale of microns (1-100s of micron)[25, 30], making it difficult to confirm the microstructure of the synthesized materials. More current literature on actinide oxalates has focused on identifying solid phases present during decomposition and calcination using thermogravimetric analysis (TGA) and high temperature x-ray diffraction[31, 32]. These works show that conversion is complete in air by 400 degrees Celsius for both thorium and plutonium, producing a number of carbonate and oxalate intermediaries as well as releasing volatiles such as water vapor, CO_2(g), and CO(g). While the mechanisms of degradation have been elucidated in recent literature, the morphology and microstructure of actinide oxides produced through oxalate decomposition, particularly for transuranic elements (Np, Pu), are largely unknown.

Unlike transuranic oxides, UO_2(s) microstructures are well-documented, particularly the formation process of such features. High-temperature annealing, commonly performed for fuel pellet production, recrystallizes UO_2(s), causing formation and migration of grain boundaries in the polycrystalline material[33-36]. Grain size after annealing is found to be a function of annealing time and temperature, with higher

temperatures and longer time producing larger grain size in the polycrystalline structure[36]. A very recent study on nanograined PuO_2(s) and ThO_2(s), produced through calcination of oxalate precursors, identified that increasing calcination temperature increased particle size, as well as decreased structural defects in the nanograined solids[37]. Microstructure in polycrystalline oxides can have effects on dissolution, such as preferential dissolution at grain boundaries, which has been reported for CeO_2(s)[38, 39], ThO_2(s)[40], and UO_2(s)[41, 42]. While grain boundary facilitated dissolution has been recently reported for NpO_2(s)[43], characterization of the effect of microstructures in NpO_2(s) and PuO_2(s) is still limited.

In light of the potential variability in microstructure based on synthesis parameters (namely, calcination temperature and time) and the potential effects of microstructure on dissolution, more systematic synthesis and characterization of the microstructure of transuranic oxides may be used explain reported actinide oxide solubility data set discrepancies. Given the recent literature on polycrystalline NpO_2(s) dissolution mechanisms[43], corresponding field studies on dissolution and transport from NpO_2(s)[44] and significant production of polycrystalline NpO_2(s) via calcination at U.S.

Department of Energy (DOE) Savannah River Site (SRS) for ^{238}Pu targets[45-47], the further characterization and dissolution of $NpO_2(s)$ has been chosen for study. ^{237}Np is a long-lived radionuclide that is found both at DOE sites, such as SRS, as well as in spent nuclear fuel[2]. While highly insoluble under reducing conditions, if oxidized, Np is highly mobile in the environment[48-50], making it a risk-driver for environmental assessment.

Experimental

$NpO_2(s)$ Synthesis

Caution: ^{237}Np is an alpha-emitting radionuclide and safe handling requires appropriate facilities and qualified personnel. These experiments were conducted in licensed laboratories at Clemson University.

$NpO_2(s)$ was synthesized via calcination of Np(IV)-oxalate. Neptunium oxalate is a commonly used precursor for $NpO_2(s)$[23, 46, 47]. While Np oxalate is typically prepared in HNO_3, synthesis was performed in HCl to maintain Np(IV) in solution without chemical reductants that could potentially alter the structure of the final $NpO_2(s)$ product. Plutonium(IV) oxalate has been reported to be prepared successfully in HCl[51],

supporting use of HCl. ^{237}Np(IV) stock was prepared by bubbling 95% N_2/5% H_2 gas through Np(V) solution in 1N HCl in the presence of powdered platinum (Pt) black catalyst (Alfa Aesar), stirring constantly for 45 minutes, similar to methods reported by Strickert et al.[52] and Nakamura et al.[53]. ^{237}Np concentration and oxidation state in the stock solution were measured using ultraviolet–visible spectroscopy (UV-VIS) and compared to reference peak locations for Np(IV) and Np(V) from Yoshida et al.[54]. The final stock solution was 100% Np(IV) and had a final concentration of 5.96 mM Np(IV) (Figure S1).

To precipitate Np(IV)-oxalate, 10 mL of the Np(IV) stock in 1N HCl was added to a 30 mL Teflon vial on a magnetic stir plate in a fume hood. The solution was constantly stirred at 500 rpm throughout the precipitation. Oxalic acid (6.67 mL, 0.25M) was added in 148 μL increments over 45 minutes to reach a final concentration of 0.1M oxalic acid in solution. Precipitation of solid was evident after approximately 20 minutes. After complete addition of oxalic acid, solution was stirred for an additional 30 minutes, then solid slurry was transferred into a 15 mL centrifuge tube and centrifuged for 10 minutes at 9000 rpm in a Beckman Coulter C1015 fixed-angle rotor to separate

out solids >100nm, according to Stoke's Law[55]. A green powder was visible at the tip of centrifuge tube (Figure S2) and was transferred into doubly contained porcelain crucibles for calcination. A small amount of the initial Np(IV)-oxalate was reserved for future characterization. Samples were allowed to air dry for approximately 1 hour before transferring into furnace.

Np(IV)-oxalate was calcined at varying temperatures, ranging from 400-900°C in a multi-segment programmable furnace (Thermo Scientific Lindberg/Blue M). The lowest selected temperature was 400°C based on Th and Pu oxalate decomposition literature, which indicates that conversion to the pure oxide phase is complete around 400°C[31, 32]. Calcination temperature was increased at 100°C intervals to provide large enough temperature steps to ensure distinct differences between samples, and 900°C was chosen as the highest temperature because most transuranic oxides (Np, Pu) are prepared at a maximum of 900-1000°C[22, 25-30, 46, 47, 56]. Though there are not studies directly with Np, no additional phases changes in ThO_2(s) and PuO_2(s) systems have been observed up to 1000 °C and thus the pure NpO_2(s) phase is expected[31, 32]. Masses of NpO_2(s) produced, as well as radiation protection limitations, prevented the

collection of XRD patterns for the NpO_2(s) used in this work. Samples were first held at 150°C for 1 hour to fully dehydrate the oxalate, then ramped at a speed of 100°C/hour to final calcination temperature (400, 500, 600, 700, 800, or 900°C). Samples were held at final temperature for 12 hours, then cooled at 100°C/hour to 25°C.

NpO_2(s) Characterization

Final calcined product was characterized using scanning transmission electron microscopy (STEM) to probe surface morphology and grain size. After calcination, solids were rinsed and suspended in ethanol, then 3 μL of NpO_2(s) suspension was casted directly onto a copper-coated lacey carbon grid (300 mesh). Excess liquid was blotted from the grid with a Kimwipe and grids were covered to prevent dust deposition and left to dry prior to analysis. A Hitachi HD2000 scanning transmission electron microscope was used for STEM imaging at an accelerating voltage of 200kV. Initial Np(IV)-oxalate was characterized using STEM in the same manner as the calcined NpO_2(s). Average grain size of NpO_2(s) was calculated from electron micrographs using ImageJ software using the measurement of the diameter of 100 grains for each temperature.

NpO_2(s) Dissolution

NpO_2(s) produced at six different calcination temperatures was dissolved in identical conditions to determine the effect of calcination temperature on dissolution. For each calcination temperature, initial mass of dry solid used in dissolution experiment was determined gravimetrically. Dissolution experiments were performed under atmospheric conditions at pH 3 in 0.1M sodium perchlorate background solution. Oxidizing conditions were selected as representative of potential environmental conditions. Given the experimental conditions, oxidative dissolution of NpO_2(s) is expected to produce Np(V) aqueous species, thus preventing demonstration of reversal in the current work. Between 1-2 mg of NpO_2(s) was dissolved in 1mL background solution over 10 weeks (kinetic data presented in Figure S3), held at 25°C and constantly stirred on an orbital shaker at 90 rpm. Initial pH and E_h of background solution were measured, then pH of each reaction was measured at each sampling event (average pH across all samples was 3.05 $\pm$ 0.02; data for all replicates in Table S1). E_h was measured over time by proxy in a stored sample of background solution. At each time point, 10μL was sampled and immediately diluted to 1mL in deionized

water, centrifuged for 10 minutes at 9000 rpm in a Beckman Coulter C1015 fixed-angle rotor to remove particles >100nm according to Stoke's Law[55]. A 0.5 mL aliquot of sample was filtered using a Pall centrifuge filter (10kDa MWCO), while the remaining sample was reserved as unfiltered. Both filtered and unfiltered sample were diluted with 2% HNO_3 for ^{237}Np concentration analysis in the aqueous phase via inductively-coupled plasma mass spectrometry (ICP-MS).

A secondary dissolution was performed after 10 weeks of initial dissolution. The aqueous phase from each reaction was removed completely and 1mL of fresh pH 3/0.1M sodium perchlorate solution was added to each reaction vessel. Samples were once again held at 25°C and constantly stirred on an orbital shaker at 90 rpm for an additional 10 weeks during this secondary dissolution. The ^{237}Np concentration was measured using ICP-MS as done in the first dissolution experiment.

Results and Discussion

$NpO_2(s)$ was calcined from Np(IV)-oxalate precursor at temperatures ranging from 400°C to 900°C. Products were characterized using scanning transmission

electron microscopy (Hitachi HD2000 at 200kV). Electron micrographs showed a strong correlation between calcination temperature and grain size of NpO_2(s). As calcination temperature of NpO_2(s) increased from 400°C to 900°C, grain size increased by more than an order of magnitude (Figures 1 & 2). At lower magnification, individual grains were not visible in the sample prepared at 400°C (Figure 1, top left). At higher magnification, individual grains were visible in all samples (Figure 2), but for samples prepared at 800°C and 900°C, a single grain takes up the entire field of view. Average grain size was calculated to be approximately 11 nm at 400°C calcination and increased to 371 nm at 900°C calcination (Table 1). While grain growth due to high temperature annealing is well-documented for UO_2(s)[33-36] and has recently been reported for calcined ThO_2(s) and PuO_2(s)[37], comparable imaging has not been previously reported for NpO_2(s). Many of the existing micrographs of NpO_2(s) and PuO_2(s) were taken at much larger spatial scales than achieved in this current work, making it possible that many of the previously reported materials had similar microstructure that were simply beyond the resolution of instrumentation.

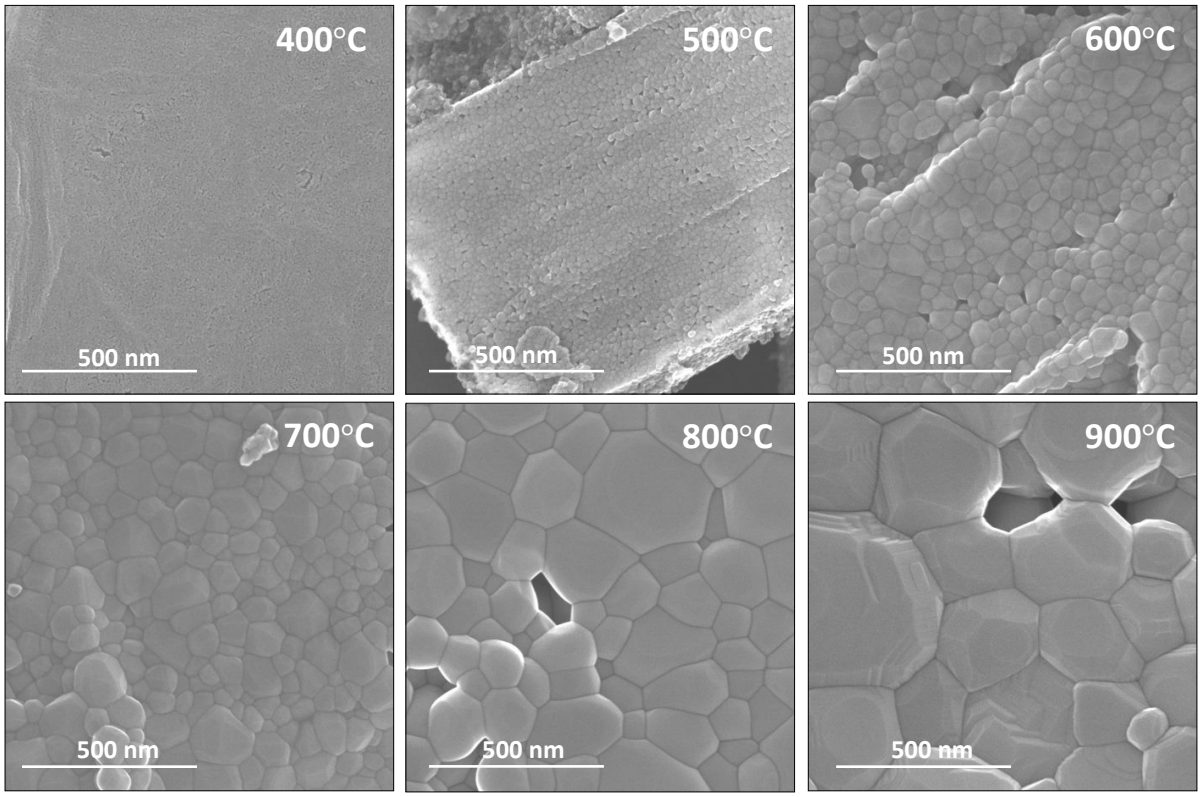

Figure 1: Scanning transmission electron micrographs of NpO_2(s) calcined at 400-900 degrees Celsius at 70.0k magnification.

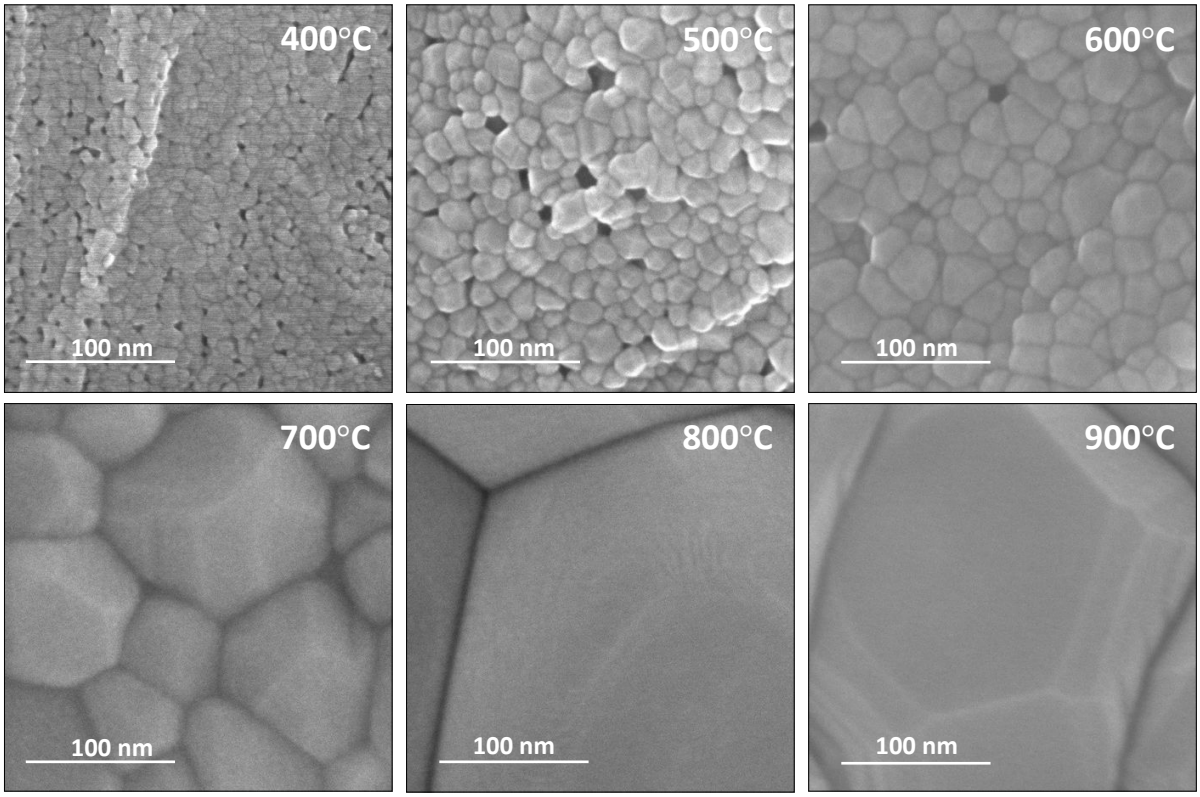

Figure 2: Scanning transmission electron micrographs of NpO_2(s) calcined at 400-900 degrees Celsius at 300.0k magnification.

Calcined NpO_2(s) materials were first dissolved over 10 weeks at 25 °C (pH 3/0.1M sodium perchlorate, showing decreased dissolution for solids calcined at higher temperature. After the initial 10 weeks, total dissolved ^{237}Np was two orders of magnitude higher for the product calcined at 400°C than for the product at 900°C (Figure 3). The logarithm of ^{237}Np concentration (molar) exhibits a linear relationship with calcination temperature (in degrees Celsius), as shown in Figure 3. Originally, we considered that the large differences in ^{237}Np concentration may be the result of an amorphous or non-crystalline phase, which is a common hypothesis for solubility differences in actinide oxide literature[3, 5, 6]. To test this hypothesis, after 10 weeks of dissolution, the aqueous phase of each reaction was removed, and the solution replaced with fresh pH 3/0.1M sodium perchlorate solution. If an amorphous phase were present on the initial material in varying quantities, dependent on calcination temperature, a secondary dissolution experiment after the initial “washing” during first 10 weeks should yield similar concentrations of total dissolved Np in all samples, regardless of calcination temperature. The secondary dissolution data shows a two-order of magnitude difference between 400°C and 900°C samples, consistent with the

trend of the first dissolution experiment, though all concentrations are approximately one order of magnitude lower than the initial dissolution. The trend in dissolution data with respect to calcination temperature is preserved, and the uniform drop in concentration in the second dissolution indicates the present of a small amount of amorphous material in all samples, regardless of calcination temperature.

Table 1: Average grain size of NpO_2(s) based on varying calcination temperature.

Calcination Temperature (°C)	**Average Grain Size (nm)**
400	11.05 ± 2.78
500	20.18 ± 5.35
600	44.77 ± 29.44
700	94.14 ± 33.90
800	213.78 ± 81.05
900	371.80 ± 126.50

Rather than varying amounts of an initial amorphous phase, the significant difference in total dissolved ^{237}Np can be attributed to free energy differences of the materials, stemming from the noticeably variant particle sizes. Smaller particle sizes, as seen in the lower calcination temperature samples (Figures 1 & 2), correspond to higher surface area and reactivity. As Navrotsky and colleagues have established for other metal oxides, particle size and surface area have a pronounced effect on surface energy of materials[12-15]. Higher surface area materials, such as nanograined solids, exhibit considerable excess surface energy, which is due, in part, to greater amount of surface defects with respect to bulk solids. The correlation between increasing calcination temperature and a decrease in surface defects has also recently been established for nanograined ThO_2(s) and PuO_2(s) using spectroscopic techniques[37]. As temperatures increase during calcination, recrystallization of NpO_2(s) decreases surface defects and increases particle size, in turn increasing the ratio of crystalline bulk to disordered surface bonds. Thus, NpO_2(s) calcined at higher temperatures, which exhibits large primary grain size, is more stable and less soluble than the nanograined solids produced at lower temperature.

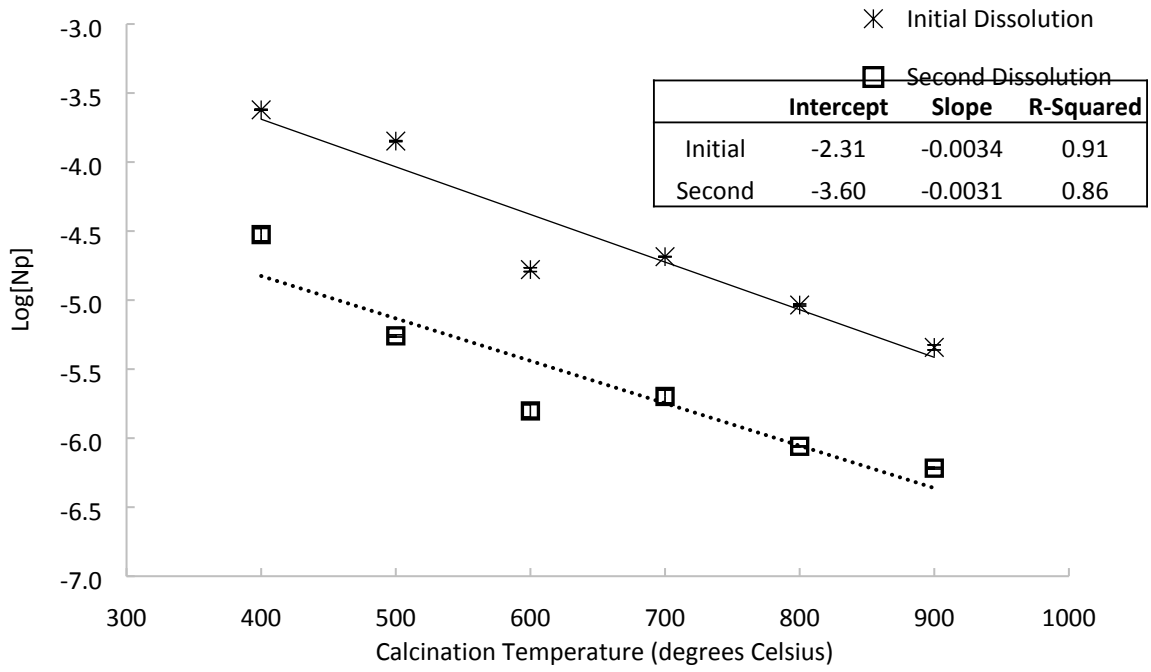

Figure 3: Aqueous log[Np] after 4 weeks of dissolution as a function of calcination temperature of NpO_2(s). Error bars are hidden by data markers.

Conclusion

NpO_2(s) produced at six temperatures, ranging from 400 to 900°C, showed grain sizes that varied from 11 to 371 nm, respectively. Subsequent aqueous dissolution data of the solids revealed that total dissolved Np varied by two orders of magnitude between 400°C and 900°C samples. Increasing calcination temperature, a relevant process condition for spent nuclear fuel reprocessing, decreased apparent solubility of NpO_2(s), which is congruent with particle size-controlled dissolution. The observed substantial increase in grain size may be due to recrystallization of the material under increasingly

high temperatures. Recrystallization may change the surface energy of the material and subsequently impact free energy of the system. There is also likely a corresponding decrease in surface area of the material at higher temperatures. This work provides unique imaging of the microstructure of NpO_2(s), along with aqueous dissolution data as a function of calcination temperature, revealing the potential for significant changes in material stability as a function of process conditions. Overall, the data indicate a need to critically evaluate existing thermodynamic data of transuranic oxides to account for potential differences in microstructure relating to calcination temperature, as well as other relevant process conditions, and to apply more advanced imaging techniques to future actinide solubility studies to address reported discrepancies in actinide oxide solubility data in the literature and potential reversibility of dissolution reactions. While this study has not measured surface energy of NpO_2(s), it suggests an urgent need for thermodynamic measurements of highly characterized transuranic oxides using high temperature melt calorimetry to elucidate the reason for observed orders of magnitude difference in dissolved ^{237}Np and provide quantitative thermodynamic data, as has been explored for other metal oxides. NpO_2(s) grain size evidently varies dramatically based on process conditions such as calcination temperature, and variation causes significant effect on dissolution, with far-reaching implications for overall stability of nuclear materials in the environment.

ASSOCIATED CONTENT

Supporting Information.

1 file with 3 figures and 1 table.

AUTHOR INFORMATION

Corresponding Author

*Brian A. Powell, bpowell@clemson.edu, office (864) 656-1004

342 Computer Court, Anderson, SC, US 29625

Author Contributions

The manuscript was written through contributions of all authors. All authors have given approval to the final version of the manuscript.

ACKNOWLEDGMENTS

This work is supported by the U.S. Department of Energy (DOE) Office of Science, Office of Basic Energy Sciences and Office of Biological and Environmental Research under Award Number DE-SC-00012530.

References

1. R. C. Ewing, Long-term storage of spent nuclear fuel, *Nature Materials*, 2015, **14**, 252.
2. J. Bruno and R. C. Ewing, Spent nuclear fuel, *Elements*, 2006, **2**, 343-349.
3. V. Neck and J. Kim, Solubility and hydrolysis of tetravalent actinides, *Radiochimica Acta*, 2001, **89**, 1-16.

4. V. Neck, J. Kim, B. Seidel, C. M. Marquardt, K. Dardenne, M. Jensen and W. Hauser, A spectroscopic study of the hydrolysis, colloid formation and solubility of Np (IV), *Radiochimica Acta*, 2001, **89**, 439-446.
5. T. Fanghänel and V. Neck, Aquatic chemistry and solubility phenomena of actinide oxides/hydroxides, *Pure and Applied Chemistry*, 2002, **74**, 1895-1907.
6. V. Neck, M. Altmaier, R. Müller, A. Bauer, T. Fanghänel and J.-I. Kim, Solubility of crystalline thorium dioxide, *Radiochimica Acta*, 2003, **91**, 253-262.
7. V. Neck, M. Altmaier and T. Fanghänel, Solubility of plutonium hydroxides/hydrous oxides under reducing conditions and in the presence of oxygen, *Comptes Rendus Chimie*, 2007, **10**, 959-977.
8. J. Fuger, Problems in the Thermodynamics of the Actinides in Relation with the Back-end of the Nuclear Fuel Cycle, *Journal of nuclear materials*, 1993, **201**, 3-14.
9. A. Navrotsky, Calorimetry of nanoparticles, surfaces, interfaces, thin films, and multilayers, *The Journal of Chemical Thermodynamics*, 2007, **39**, 1-9.
10. A. Navrotsky, High-temperature oxide melt calorimetry of oxides and nitrides, *The Journal of Chemical Thermodynamics*, 2001, **33**, 859-871.
11. A. Navrotsky, Progress and new directions in high temperature calorimetry revisited, *Physics and Chemistry of Minerals*, 1997, **24**, 222-241.
12. A. Navrotsky, L. Mazeina and J. Majzlan, Size-driven structural and thermodynamic complexity in iron oxides, *Science*, 2008, **319**, 1635-1638.
13. A. Navrotsky, Nanoscale Effects on Thermodynamics and Phase Equilibria in Oxide Systems, *ChemPhysChem*, 2011, **12**, 2207-2215.
14. N. Birkner and A. Navrotsky, Thermodynamics of manganese oxides: Effects of particle size and hydration on oxidation-reduction equilibria among hausmannite, bixbyite, and pyrolusite, *American Mineralogist*, 2012, **97**, 1291-1298.
15. X. Guo, D. Wu, S. V. Ushakov, T. Shvareva, H. Xu and A. Navrotsky, Energetics of hydration on uranium oxide and peroxide surfaces, *Journal of Materials Research*, 2019, **34**, 3319-3325.
16. S. Nakayama, T. Yamaguchi and K. Sekine, Solubility of neptunium (IV) hydrous oxide in aqueous solutions, *Radiochimica acta*, 1996, **74**, 15-20.
17. H. Moriyama, M. I. Pratopo and K. Higashi, The solubility and colloidal behaviour of neptunium (IV), *Science of the total environment*, 1989, **83**, 227-237.
18. D. Rai and J. L. Ryan, Neptunium (IV) hydrous oxide solubility under reducing and carbonate conditions, *Inorganic Chemistry*, 1985, **24**, 247-251.
19. D. Rai, J. Swanson and J. Ryan, Solubility of $NpO_2 \cdot xH_2O$ (am) in the presence of Cu (I)/Cu (II) redox buffer, *Radiochimica Acta*, 1987, **42**, 35-42.
20. B. A. Powell, Z. Dai, M. Zavarin, P. Zhao and A. B. Kersting, Stabilization of plutonium nano-colloids by epitaxial distortion on mineral surfaces, *Environmental science & technology*, 2011, **45**, 2698-2703.
21. L. Soderholm, P. M. Almond, S. Skanthakumar, R. E. Wilson and P. C. Burns, The structure of the plutonium oxide nanocluster $[Pu_{38}O_{56}Cl_{54}(H_2O)_8]^{14-}$, *Angewandte Chemie International Edition*, 2008, **47**, 298-302.
22. J. Facer Jr and K. Harmon, *Precipitation of plutonium (IV) oxalate*, Hanford Atomic Products Operation, Richland, WA (United States), 1954.
23. J. Porter, Production of Neptunium Dioxide, *Industrial & Engineering Chemistry Process Design and Development*, 1964, **3**, 289-292.

24. D. T. Rankin and G. Burney, *Particle size of $^{238}PuO_2$ obtained by oxalate precipitation and calcination*, Du Pont de Nemours (EI) and Co., Aiken, SC (USA). Savannah River Lab., 1974.
25. P. Smith, G. Burney, D. Rankin, D. Bickford and R. Sisson Jr, *Effect of oxalate precipitation on PuO_2 microstructures*, Du Pont de Nemours (EI) and Co., 1976.
26. G. White, L. Bray and P. Hart, Optimization of thorium oxalate precipitation conditions relative to derived oxide sinterability, *Journal of Nuclear Materials*, 1981, **96**, 305-313.
27. G. A. Burney, *Controlled PuO_2 particle size from Pu (III) oxalate precipitation*, EI du Pont de Nemours & Company, Savannah River Laboratory, 1984.
28. V. Tyrpekl, M. Beliš, T. Wangle, J. Vleugels and M. Verwerft, Alterations of thorium oxalate morphology by changing elementary precipitation conditions, *Journal of Nuclear Materials*, 2017, **493**, 255-263.
29. T. Wangle, V. Tyrpekl, S. Cagno, T. Delloye, O. Larcher, T. Cardinaels, J. Vleugels and M. Verwerft, The effect of precipitation and calcination parameters on oxalate derived ThO_2 pellets, *Journal of Nuclear Materials*, 2017, **495**, 128-137.
30. X. Machuron-Mandard and C. Madic, Plutonium dioxide particle properties as a function of calcination temperature, *Journal of alloys and compounds*, 1996, **235**, 216-224.
31. N. Vigier, S. Grandjean, B. Arab-Chapelet and F. Abraham, Reaction mechanisms of the thermal conversion of Pu (IV) oxalate into plutonium oxide, *Journal of Alloys and Compounds*, 2007, **444**, 594-597.
32. N. Raje and A. Reddy, Mechanistic aspects of thermal decomposition of thorium oxalate hexahydrate: a review, *Thermochimica Acta*, 2010, **505**, 53-58.
33. R. Scott, A. R. Hall and J. Williams, The plastic deformation of uranium oxides above 800° C, *Journal of Nuclear Materials*, 1959, **1**, 39-48.
34. H. Hallberg and Y. Zhu, Stability of grain boundary texture during isothermal grain growth in UO_2 considering anisotropic grain boundary properties, *Journal of Nuclear Materials*, 2015, **465**, 664-673.
35. T. E. Chung and T. J. Davies, The superplastic creep of uranium dioxide, *Journal of Nuclear Materials*, 1979, **79**, 143-153.
36. J. B. Ainscough, B. W. Oldfield and J. O. Ware, Isothermal grain growth kinetics in sintered UO_2 pellets, *Journal of Nuclear Materials*, 1973, **49**, 117-128.
37. L. Bonato, M. Virot, T. Dumas, A. Mesbah, E. Dalodière, O. D. Blanco, T. Wiss, X. Le Goff, M. Odorico and D. Prieur, Probing the local structure of nanoscale actinide oxides: a comparison between PuO_2 and ThO_2 nanoparticles rules out PuO_{2+x} hypothesis, *Nanoscale Advances*, 2020, **2**, 214-224.
38. C. L. Corkhill, D. J. Bailey, F. Y. Tocino, M. C. Stennett, J. A. Miller, J. L. Provis, K. P. Travis and N. C. Hyatt, Role of microstructure and surface defects on the dissolution kinetics of CeO_2, a UO_2 fuel analogue, *ACS applied materials & interfaces*, 2016, **8**, 10562-10571.
39. C. L. Corkhill, E. Myllykylä, D. J. Bailey, S. M. Thornber, J. Qi, P. Maldonado, M. C. Stennett, A. Hamilton and N. C. Hyatt, Contribution of energetically reactive surface features to the dissolution of CeO_2 and ThO_2 analogues for spent nuclear fuel microstructures, *ACS applied materials & interfaces*, 2014, **6**, 12279-12289.
40. J. Vandenborre, B. Grambow and A. Abdelouas, Discrepancies in thorium oxide solubility values: study of attachment/detachment processes at the solid/solution interface, *Inorganic chemistry*, 2010, **49**, 8736-8748.

41. D. J. Wronkiewicz, E. C. Buck and J. K. Bates, Grain Boundary Corrosion and Alteration Phase Formation During the Oxidative Dissolution of UO_2 Pellets, *MRS Online Proceedings Library Archive*, 1996, **465**.
42. D. J. Wronkiewicz, J. K. Bates, S. F. Wolf and E. C. Buck, Ten-year results from unsaturated drip tests with UO_2 at 90 C: implications for the corrosion of spent nuclear fuel, *Journal of Nuclear Materials*, 1996, **238**, 78-95.
43. K. M. Peruski, K. C. Koehler and B. A. Powell, Grain Boundary Facilitated Dissolution of Nanocrystalline NpO_2(s) from Legacy Waste Processing, *Environmental Science: Nano*, 2020, DOI: https://doi.org/10.1039/D0EN00262C.
44. K. M. Peruski, M. Maloubier, D. I. Kaplan, P. M. Almond and B. A. Powell, Mobility of Aqueous and Colloidal Neptunium Species in Field Lysimeter Experiments, *Environmental Science & Technology*, 2018, **52**, 1963-1970.
45. R. E. Myrick and R. L. Folger, Fabrication of Targets for Neutron Irradiation of Neptunium Dioxide, *Industrial & Engineering Chemistry Process Design and Development*, 1964, **3**, 309-313.
46. J. Duffey, *Lab Scale Production of NpO_2*, SRS (US). Funding organisation: US Department of Energy (United States), 2003.
47. J. Duffey, *Characterization of Neptunium Oxide Generated Using the HB-Line Phase II Flowsheet*, SRS, 2003.
48. J. P. Kaszuba and W. H. Runde, The aqueous geochemistry of neptunium: Dynamic control of soluble concentrations with applications to nuclear waste disposal, *Environmental Science & Technology*, 1999, **33**, 4427-4433.
49. R. Silva and H. Nitsche, Actinide environmental chemistry, *Radiochimica acta*, 1995, **70**, 377-396.
50. G. Choppin, Actinide speciation in the environment, *Journal of Radioanalytical and Nuclear Chemistry*, 2007, **273**, 695-703.
51. W. Runde, L. F. Brodnax, G. Goff, A. C. Bean and B. L. Scott, Directed synthesis of crystalline plutonium (III) and (IV) oxalates: accessing redox-controlled separations in acidic solutions, *Inorganic chemistry*, 2009, **48**, 5967-5972.
52. R. G. Strickert, D. Rai and R. W. Fulton, 1983.
53. T. Nakamura, M. Takahashi, T. Fukasawa and M. Utamura, c, *Journal of Nuclear Science and Technology*, 1992, **29**, 393-395.
54. Z. Yoshida, S. G. Johnson, T. Kimura and J. R. Krsul, in *The Chemistry of the Actinide and Transactinide Elements*, eds. L. R. Morss, N. M. Edelstein and J. Fuger, Springer, The Netherlands, Fourth edn., 2010, vol. 2, ch. 6, pp. 699-812.
55. M. L. Jackson, *Soil chemical analysis: Advanced course*, UW-Madison Libraries Parallel Press, 2005.
56. G. L. Silver, *Plutonium oxalates as sources of plutonium dioxide*, Los Alamos National Lab.(LANL), Los Alamos, NM (United States), 2010.

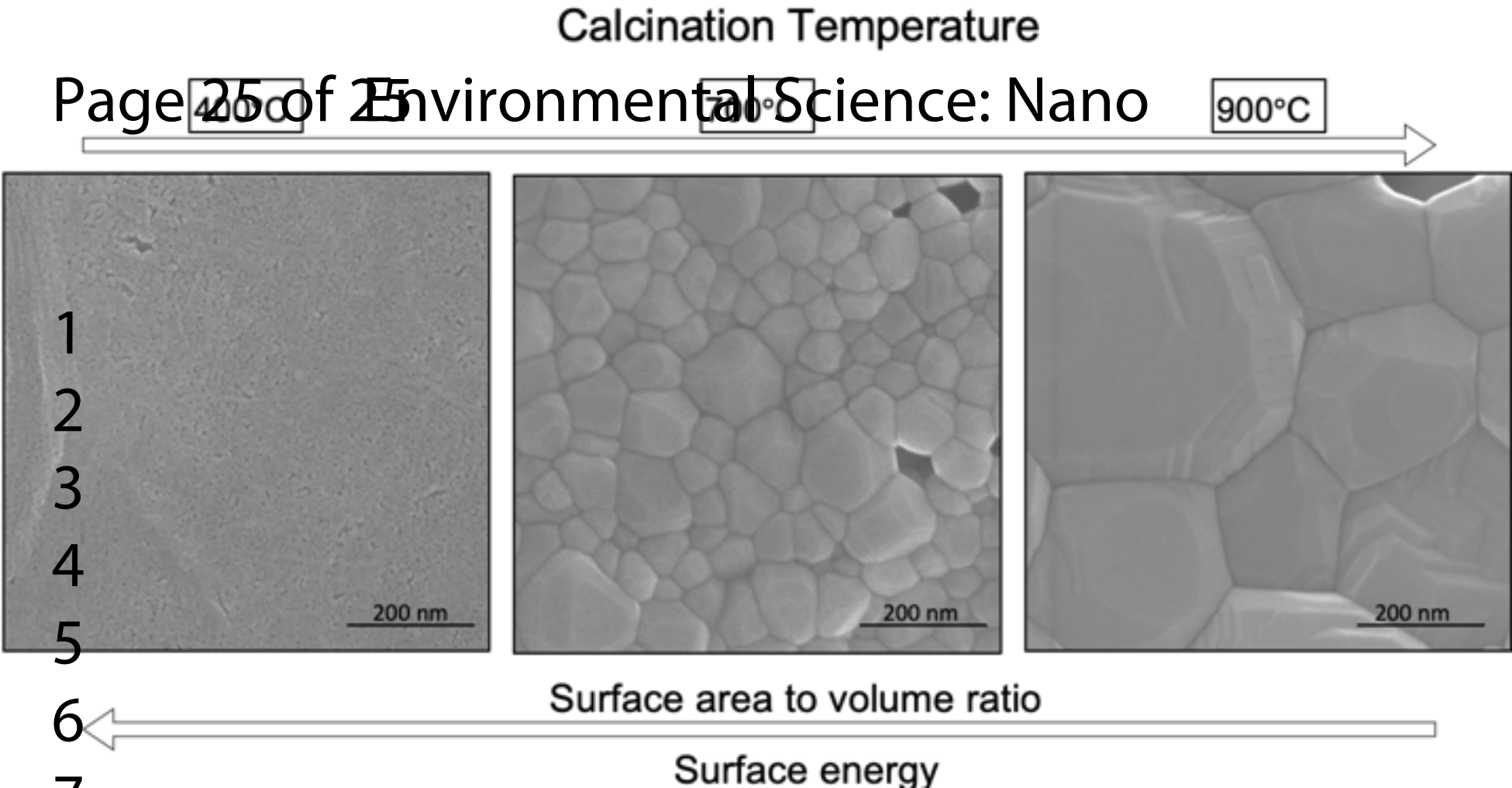
Calcination Temperature
400°C
700°C
900°C
200 nm
200 nm
200 nm
Surface area to volume ratio
Surface energy